

Dynamics of Templated Assembly of Nanoparticle Filaments within Nanochannels

Ermanno Miele, Sanoj Raj, Zhaslan Baraissov, Petr Král, and Utkur Mirsaidov*

Nanoparticles (NPs) can self-assemble into complex, organized superstructures on patterned surfaces through fluid-mediated interactions. However, the detailed mechanisms for such NP assemblies are largely unknown. Here, using in situ transmission electron microscopy, the stepwise self-assembly dynamics of hydrophobic gold NPs into long filaments formed on the surfaces of water-filled patterned nanochannel templates is observed. First, the formation of a meniscus between the nanochannel walls, during the slow drying of water, causes accumulation of the NPs in the middle of the nanochannels. Second, owing to the strong van der Waals attraction between the NP ligands, the NPs condense into filaments along the centers of the nanochannels. Filaments with highly fluctuating longitudinal NP densities are also observed to fragment into separated structures. Understanding the intermediate stages of fluid-mediated NP self-assembly on patterned surfaces will have important implications for the controlled formation of templated NP assemblies with numerous applications.

Self-assembly of nanoparticles (NPs) is an important bottom-up nanofabrication method in which NPs spontaneously organize into ordered superstructures.^[1–3] The collective behavior of NPs in assemblies leads to optical, electronic, and mechanical

Dr. E. Miele, Z. Baraissov, Prof. U. Mirsaidov
Department of Physics
National University of Singapore
Singapore 117551, Singapore
E-mail: mirsaidov@nus.edu.sg


Dr. E. Miele, Z. Baraissov, Prof. U. Mirsaidov
Centre for Bioimaging Sciences and Department of Biological Sciences
National University of Singapore
Singapore 117557, Singapore

Dr. E. Miele, Z. Baraissov, Prof. U. Mirsaidov
Centre for Advanced 2D Materials and Graphene Research Centre
National University of Singapore
Singapore 117546, Singapore

S. Raj, Prof. P. Král
Department of Chemistry
University of Illinois at Chicago
Chicago, IL 60607, USA

Z. Baraissov, Prof. U. Mirsaidov
NUSNNI-NanoCore
National University of Singapore
Singapore 117411, Singapore

Prof. P. Král
Department of Physics
Department of Biopharmaceutical Sciences
University of Illinois at Chicago
Chicago, IL 60607, USA

 The ORCID identification number(s) for the author(s) of this article can be found under <https://doi.org/10.1002/adma.201702682>.

DOI: 10.1002/adma.201702682

properties that are distinct from those of the bulk materials and individual NPs.^[3,4] These uniquely engineered properties make NP assemblies attractive candidates for biosensing,^[5,6] plasmonic,^[7,8] catalytic,^[9,10] and photovoltaic applications.^[11,12] For instance, NP assemblies with a precisely defined interparticle spacings and periodicities result in superstructures that can support quasi-loss-free transmission of electromagnetic fields in the form of plasmonic waveguides, which are needed for future high-speed optoelectronic devices.^[13–15]

NP self-assembly within solutions is driven by intermolecular forces between NPs and external forces.^[2,16,17] Hydrophobic,^[18] van der Waals (vdW),^[19] and electrostatic interactions^[20] between NPs

are typical intermolecular forces that guide NP self-assembly. Externally applied electrical,^[21] magnetic,^[22] and fluidic forces^[23] can also drive or affect NP self-assembly.

Alternatively, templated assemblies of NPs, which use molecular linkers^[24] as well as hard^[25] and soft^[26,27] nanoscale materials as templates for NP ordering, offer additional possibilities to control NP organization in these assemblies. For example, NP self-assembly induced by capillary forces acting on NPs on top of a patterned surface serving as an assembly template has potential application in high-throughput, large-scale nanofabrication.^[28–34] The mechanistic understanding of templated NP self-assemblies in solutions, especially on templated surfaces, is rather limited^[35] because of the experimental challenges associated with direct visualization of nanoscale processes in liquids. Therefore, fluid-mediated NP assemblies are characterized only post-assembly^[34] using a “quench and look” approach^[36] and optical methods.^[37,38] However, these methods cannot reveal the details about intermediate stages of NP self-assembly processes. Our objective is to understand how templated substrates drive the assembly of NPs. Specifically, we are interested in the detailed mechanisms of NP assemblies inside nanochannels.

In situ liquid-cell transmission electron microscopy (LC-TEM)^[39–43] allows studying the detailed interactions between NPs and their self-assembly dynamics.^[44–52] Here, using in situ LC-TEM, we directly observed the self-assembly dynamics of NP filaments from aqueous suspensions of hydrophobic-coated gold NPs inside the patterned nanochannels. Our experimental liquid cell platform consisted of two electron-translucent SiN_x membranes (Figure 1A–B) sandwiching and isolating a solution of gold NPs from the TEM vacuum. The nanochannels were

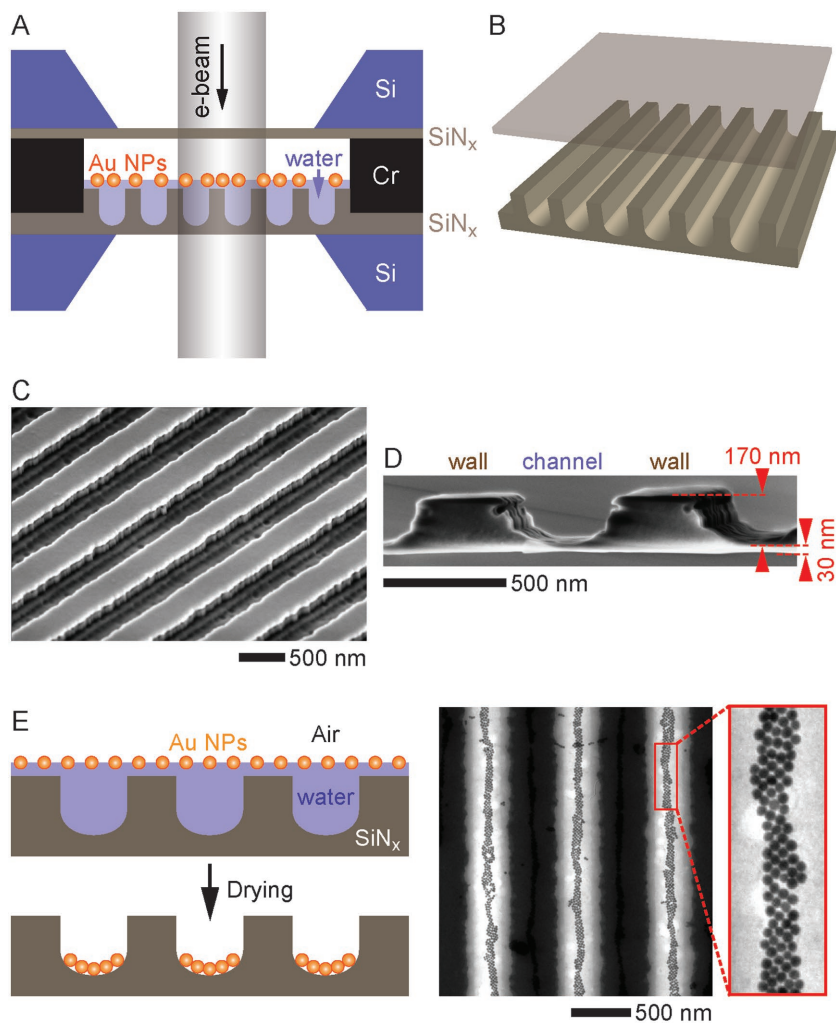


Figure 1. Nanochannel platform for in situ TEM experiments. A, B) Schematics of the liquid cell with patterned nanochannels. Two silicon nitride (SiN_x) membranes sandwich a solution of hydrophobic gold nanoparticles (NPs). The top SiN_x membrane window is 30-nm thick. C) Top-down and D) cross-sectional scanning electron microscopy (SEM) images of the bottom membrane with patterned nanofluidic channels. An array of ≈ 170 -nm deep and ≈ 200 -nm wide nanochannels with a pitch of 850 nm are patterned on this bottom membrane. E) Gold NPs in an aqueous solution applied to the nanochannels assemble into quasi-1D NP monolayers upon drying the water.

fabricated directly on the bottom SiN_x membrane of the liquid cell (Figure 1C–D), which was plasma treated before loading the NP suspension and in situ TEM imaging (Section S1, Supporting Information). Plasma treatment rendered the nanochannel surfaces hydrophilic and ensured that the nanochannels retained water. The top membrane of the liquid cell was made hydrophobic by coating with 1H, 1H, 2H, 2H-perfluorooctyltriethoxysilane (POTS). This hydrophobicity prevented the top membrane from wetting and ensured that the NP solution between the two membranes was confined to the bottom membrane containing nanochannels. An aqueous suspension of hydrophobic gold NPs was loaded into the liquid cell, which was then placed into a holder and inserted into the TEM for imaging (Figure 1A). We chose to use hydrophobic gold NPs coated with alkyl acrylate ligands because this ensures that the NPs accumulate at the water–air interface and prevent

the adsorption of the buoyant NPs onto the bottom membrane.

Visualization of the NP suspensions drop-cast and dried under ambient conditions on the nanochannel membrane revealed that the NPs sedimented inside the nanochannels, forming quasi-1D NP monolayers resembling straight chains (Figure 1E). The volume of each channel was extremely small ($V_{\text{channel}} \approx 0.5 (\pi R^2 L) = 0.5 (\pi \times (200 \text{ nm})^2 \times 175 \mu\text{m}) \approx 11 \text{ fL}$, $R \approx 200 \text{ nm}$, $L \approx 175 \mu\text{m}$), which dries out rapidly under the ambient conditions. This rapid drying causes the NPs to sediment at the bottom of the nanochannels before the NPs can self-assemble via short-range intermolecular forces. To explore the NP assembly modes under slow-drying conditions, we studied their templated assembly inside a hermetically sealed liquid cell using in situ TEM imaging (Figure 1A).

Figure 2 shows the real-time assembly dynamics of the hydrophobic gold NPs upon drying of a water-filled nanochannel (Video S1, Supporting Information). In the initial stages of drying, a meniscus forms between the two hydrophilic walls of the nanochannel, and the NPs concentrate at the center of the nanochannel and accumulate at the bottom of the meniscus (Figure 2: $t = 0.0$ –35.9 s). Next, these NPs form a thin NP filament through their gradual attachment (Figure 2: $t = 62.9$ s). When the water starts to dry along the channel, this flexible NP filament bends and coils due to the dragging by the three-phase contact line of the receding water front (Figure 2: $t = 67.7$ –77.3 s).

To better understand the NP self-assembly dynamics and further explore if the NPs can assemble into thicker and more robust filaments that remain intact during assembly, we increased the NP concentration loaded into the liquid cell from $\approx 4 \times 10^{13}$ NPs mL^{-1} to $\approx 1 \times 10^{14}$ NPs mL^{-1} . Here, similar to our

observations in Figure 2, the slight drying of water and the subsequent meniscus formation between the walls of the nanochannel induced the migration of the NPs toward the center of the nanochannel, where the NPs accumulated and assembled into a micrometer-long filament through their mutual attachment (Video S2, Supporting Information). This NP motion is initiated by the repulsion of the hydrophobic NPs by the hydrophilic nanochannel walls (i.e., hydrophilic surfaces repelling hydrophobic objects). In the initial stages of the NP assembly, this NP motion, causing the subsequent accumulation in the center of the nanochannel, was quite rapid (Figure 3A: $t = 0.0$ –29.0 s). As the density of the NPs in the center of the channel increased and the NPs came closer into mutual contact, their motion toward each other slowed but did not fully stop (Figure 3A: $t = 45.0$ –66.9 s, Figure 3C). The NP filament continued to further compress sideways into a tight filament until its diameter

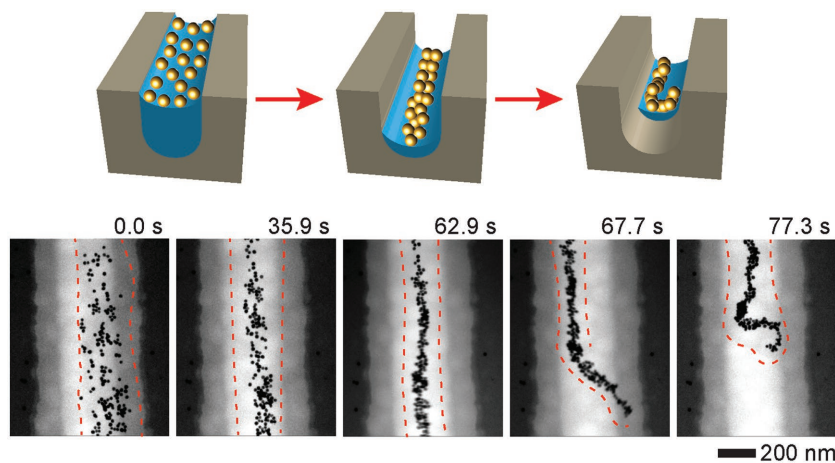


Figure 2. In situ TEM image series of the hydrophobic NP assembly in the center of the nanochannel. As the liquid in the nanochannel dries and a meniscus forms between two walls of the nanochannel, the NPs concentrate in the center of the nanochannel, and the NPs accumulate at the bottom of the water meniscus ($t = 0.0$ – 62.9 s). When the water starts to dry along the length of the nanochannel, the three-phase contact line (water-SiN_x membrane-air) drags the assembled NP filament along the length of the channel in the direction of the receding liquid, causing the filament to coil ($t = 67.7$ – 77.3 s). The dashed red lines indicate the boundary of the liquid (three-phase contact line) inside the nanochannel. Here, the areal density of the buoyant NPs inside the channel at $t = 0$ s is ≈ 200 NPs μm^{-2} .

reached ≈ 80 nm, at which point the self-assembly of the filament ceased (Figure 3A: $t = 100.6$ s) (Video S2, Supporting Information). Notably, during the assembly, the NPs continued to compress even when the channel was not fully dry. In fact, when water spontaneously returns to partially fill the channel, the filament retained its structure (Figure 3A: $t = 120.5$ s).

The accumulation of the hydrophobic NPs at the bottom of the meniscus was caused by repulsion from the highly curved water surface at the hydrophilic channel walls. However, the origin of the gradual NP self-assembly, followed by tight packing into filaments, is more intriguing, as these buoyant NPs interact through vdW, electrostatic, hydrophobic, steric, and other forces. The NP chemistry does not allow for charging (Section S2, Supporting Information), which at most will delay their final approach. Therefore, we believe that at longer distances, the NPs interact by weak vdW forces between the NP gold cores and hydrophobic forces. As the NPs become closer, the NPs attract by rather strong vdW coupling up to a distance limited by the steric forces. In bulk solutions, the vdW attractions between NP gold cores create a dominant, albeit rather weak, force due to the core separation by ligands. For buoyant hydrophobic NPs on water, approximately two third of the NP surface is exposed to air, and therefore, the interaction (mostly ligand–ligand vdW coupling) between the exposed ligands of nearby NPs becomes very large at close distances. When the NPs are fully submerged in a bulk solution, the vdW coupling between ligands typically results in weaker forces (due to compensation by ligand–solvent interactions).

To test this hypothesis, we used atomistic molecular dynamics (MD) simulations to model the interactions between two electrically neutral dodecyl-acrylate-coated 7.8 nm gold NPs (Figure 3D). The vdW interactions between the NPs accounting for the gold

cores and ligands (including steric repulsion) were separately considered (Section S3, Supporting Information). The initial center-to-center spacing between the NPs was set to ≈ 10.6 nm (Figure 3D). When the cut-off distance for the ligand–ligand vdW coupling was set to 1 nm, the largely exposed NPs did not come any closer after a 10-ns simulation. However, when the cut-off distance was set to 2 nm, within 3 ns, the NPs attached through the interaction between their ligands, and their center-to-center distance reduced to 9.4 nm (Section S3 and Video S3, Supporting Information). The calculated net interaction energy between the two dodecyl-acrylate-coated and tightly coupled NPs was $\approx 250 k_B T$ at the attachment point, while the contribution of the core–core vdW attraction was only $\approx 6 k_B T$. These results show that attraction due to the ligand–ligand vdW coupling plays an important role in the gradual adhesion of the NPs into compact filaments. This NP adhesion is consistent with our observation of sideways compression of the NP filament, which occurred after the drying-induced accumulation in the center of the nanochannel.

The ability to directly visualize the formation of NP assemblies allows us to explore the possible failure modes that may occur during NP self-assembly, which may result in fragmented NP filaments. Figure 4 shows a NP filament undergoing fragmentation during drying-mediated self-assembly (Video S4, Supporting Information). An area with a low local density of NPs within the nanochannel prevented the complete attachment between two densely packed NP regions, and therefore, these regions failed to link together (Figure 4: $t = 34.2$ s), eventually forming two discrete filament fragments. These two filament fragments receded in opposite directions in the nanochannel as the water starts to dry (Figure 4: $t = 50.0$ – 112.4 s).

In summary, the direct nanoscale observation in real-time revealed the dynamics of NP self-assembly inside templated nanochannels to give rise to robust NP filaments. The drying of water within the channel formed a meniscus between the channel sidewalls, driving the NPs toward the bottom of the meniscus in the center of the nanochannel. Here, the NPs were attracted by hydrophobic forces and interconnected into tightly attached filaments via strong ligand–ligand vdW forces between the NPs. Our approach integrating patterned surfaces with in situ liquid cell TEM imaging allows to probe the intermediate steps of various templated assemblies, which has broad significance for numerous technological applications. Patterned nanochannels on thin membranes can also serve as potential platforms to study dynamics of nanoscale chemical and physical processes under confinement.

Experimental Section

Liquid-Cell Fabrication and Assembly: The liquid cell was assembled from the top and bottom Si chips (2.6 mm \times 2.6 mm), and each chip had a small (≈ 30 μm \times 200 μm) SiN_x membrane in the center.

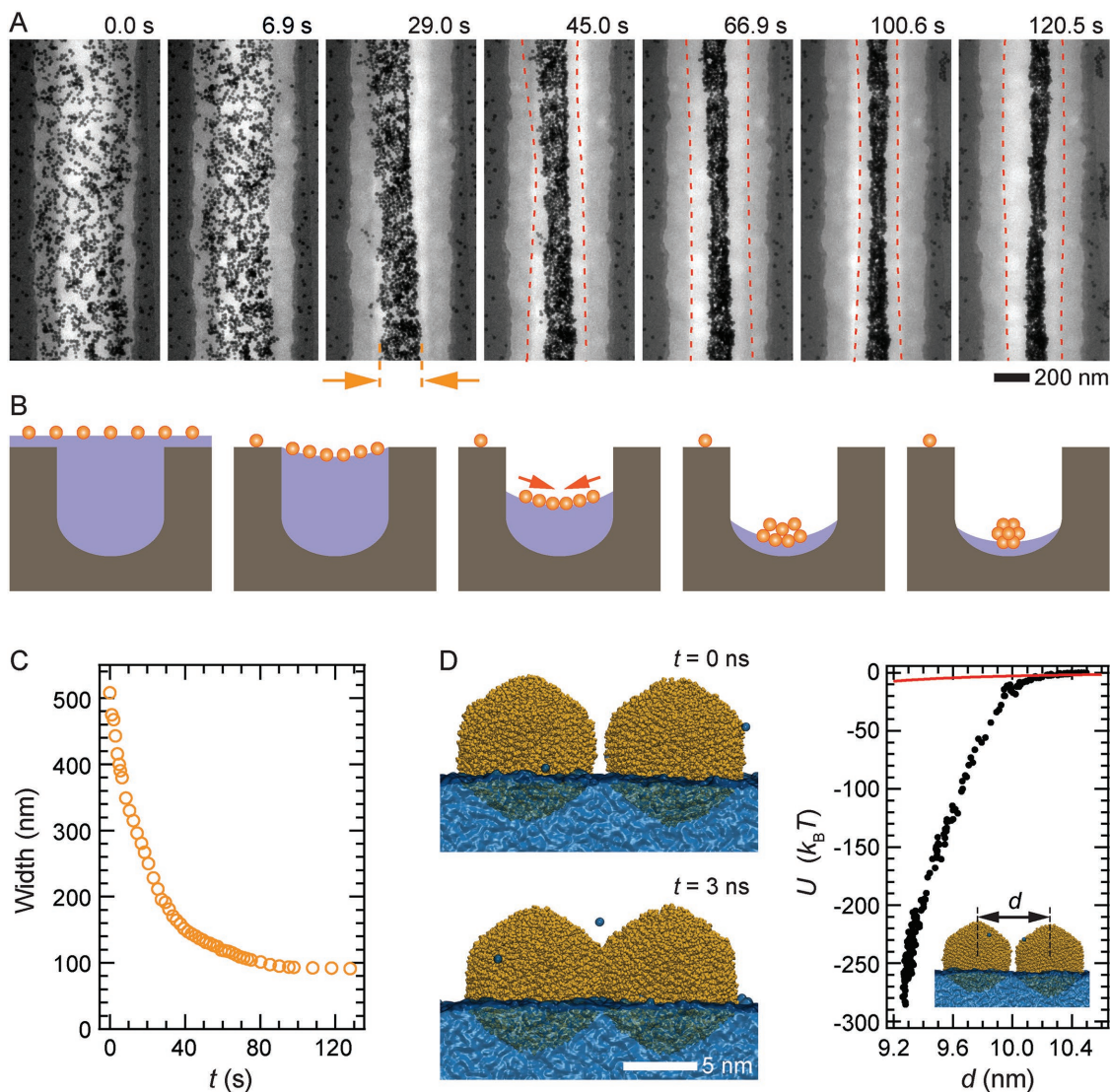


Figure 3. Fluid-assisted NP-filament formation. A) In situ TEM image series showing the filament formation (Video S2, Supporting Information). Initially, the hydrophobic gold NPs are randomly dispersed on the top of the fluid ($t = 0.0$ s). Here, the areal density of NPs inside the channel at $t = 0$ s is ≈ 1100 NPs μm^{-2} . As the liquid dries and a meniscus begins to form, the NPs migrate to the bottom of the water meniscus at the center of the nanochannel ($t = 6.9$ – 45.0 s). As the NPs come together, they contact and attach to form a robust filament ($t = 66.9$ – 120.5 s). The dashed red lines indicate the boundary of the fluid (three-phase contact line) inside the nanochannel. B) Schematic depicting the assembly of a filament. C) Projected width of the NP filament shown in (A) as a function of time, which displays that the initial aggregation of the NPs in the center proceeds rapidly and then slows and comes to a halt when the NPs are packed tightly together to form a filament. D) Left: MD simulation showing the attachment of the buoyant dodecyl-acrylate-coated NPs in water through ligand–ligand interactions (Video S3, Supporting Information). The contact angle between each NP and water is $\approx 135^\circ$. Right: The interaction energies between the two gold NPs. The strength of net interaction accounting for both the vdW coupling between the gold cores and ligand–ligand coupling (with strong ligand–ligand vdW contribution) are plotted by solid black circles. The red curve plots the strength of the vdW interaction between the gold cores of the NPs.

The bottom chip of the liquid cell had an array of 200-nm-wide and 170-nm-deep nanochannels with a pitch length of 850 nm etched into the 200-nm-thick membrane surface. The top chip of the liquid cell had a 30-nm-thick flat SiN_x membrane window with a lateral dimension of $\approx 30 \times 200 \mu\text{m}^2$ patterned in the middle. The fabrication processes of both the bottom and top chips are described in detail in Section S1 in the Supporting Information. To fabricate the chips that comprised the liquid cells, we used 4-inch double-side-polished 200- μm -thick (100) Si wafers with a SiN_x film deposited on both faces of the wafer using low-pressure chemical vapor deposition. The thickness of SiN_x on the wafers used for the top and bottom chips was 30 and 200 nm, respectively. The free-standing central SiN_x membranes and grooves

for dicing the chips were patterned on one face of the wafer using standard optical lithography. Then, the patterned SiN_x was removed by deep reactive ion etching (DRIE), exposing the bulk Si underneath. Next, the exposed bulk Si was etched with KOH solution, which created grooves on the etched face of the wafer and released the free-standing SiN_x membranes on the opposite side of the wafer. To keep the top and bottom membranes separated during the assembly and to ensure a thin layer of liquid between the membranes, 50-nm-thick Cr spacers was patterned on the membrane side of the top chip using a lift-off process.

The bottom chips were fabricated on 4-inch double-side-polished 200- μm -thick (100) Si wafers with 200-nm-thick SiN_x films on both sides. A 35-nm-thick Cr film was deposited on one face of the wafer

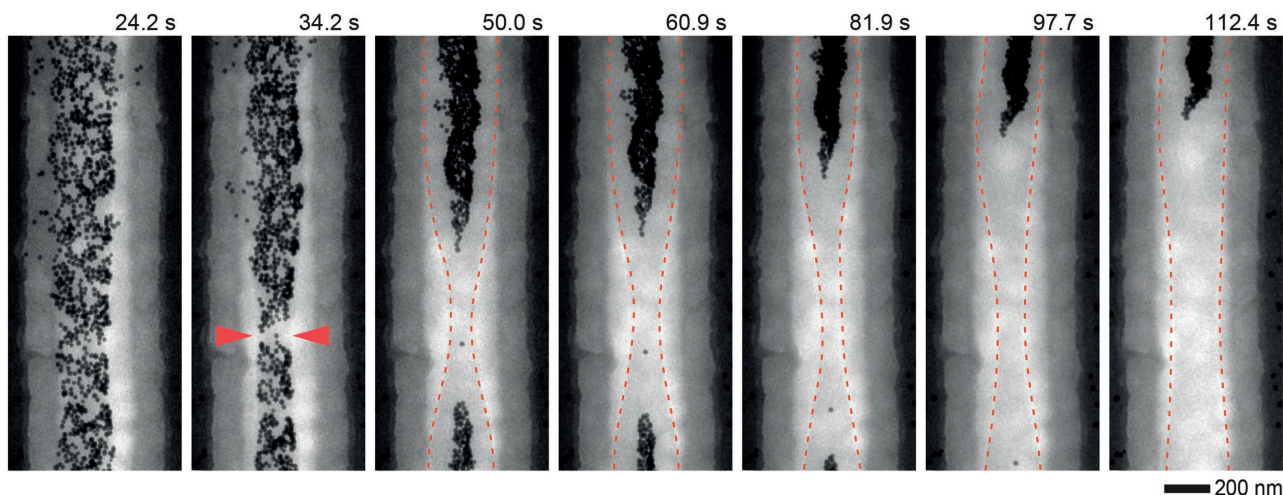


Figure 4. In situ TEM image series showing the failure mode during the assembly of the NP filament. During the drying-mediated accumulation of the NPs in the center of the nanochannel, the spontaneous formation of local low-density NP region (red arrows, $t = 34.2$ s) results in fragmentation before filament formation (Video S4, Supporting Information). Two filament fragments that failed to link move in opposite directions as water in the nanochannel further dries ($t = 50.0$ – 112.4 s). Here, the areal density of NPs inside the channel at $t = 0$ s is ≈ 800 NPs μm^{-2} .

and an e-beam resist (poly(methyl methacrylate) (PMMA), A4, 950 kDa, MicroChem Corp., Newton, MA, USA) was spin coated on top of this Cr film. On the same face of the wafer with deposited Cr, nanochannel arrays were defined on a resist using e-beam lithography. The patterned SiN_x was exposed by a Cr etch-back process. Next, on the opposite face of the wafer, membrane windows and dicing groves were patterned in a similar way as for the top chips described above. During the patterning of the membranes, the membrane patterns were aligned with the corresponding patterns of the nanochannel arrays (i.e., membranes of 775 chips were aligned with 775 arrays of nanochannels on each wafer). Then, using DRIE, we produced nanochannels in free-standing membranes by etching 170 nm of exposed SiN_x . Afterward, we removed the residual resist and Cr with acetone and a Cr etchant, respectively. Finally, the top and bottom chips were diced and cleaned (oxygen plasma and acetone–isopropyl alcohol–water washing), and the individual chips were stored in a dry box.

Sample Preparation: The membrane sides of both the top and bottom chips were cleaned with an oxygen plasma (150 W, 15 min, 25 sccm O_2 , 5 sccm Ar) and a standard wet-cleaning process (acetone, isopropyl alcohol, and deionized water). Before the final assembly of the liquid cells prior to each experiment, the top chips were coated with silane (POTS, Cat.# 667420, Sigma–Aldrich Co. LLC, St. Louis, MO, USA) using vapor-phase deposition to ensure that the top membrane was hydrophobic.^[53] Then, to render the SiN_x membrane surface of the bottom chip containing nanochannels hydrophilic, the membrane side of the chip was plasma cleaned. The hydrophilic bottom chip (contact angle of water on the SiN_x membrane is $\approx 16^\circ$)^[42] was then placed into a TEM flow holder (Hummingbird Scientific, Lacey, WA, USA). Next, a $\approx 300 \pm 100$ nL solution of 10-nm alkyl-acrylate-coated gold NPs pipetted on the bottom chip formed a thin-layer NP solution on the SiN_x membrane. The liquid cell was then sealed with the hydrophobic top chip while ensuring overlap between both the top and bottom membranes. Then, the flow holder was loaded into the TEM for in situ imaging. A 30-cm-long tube with an inner diameter of 100 μm connected the solution in the sealed liquid cell to the ambient atmosphere, which ensured that the solution inside the cell dried very slowly. The solution of alkyl-acrylate-coated gold NPs used in our experiments was prepared by diluting a stock NP solution ($\approx 7.8 \times 10^{14}$ NPs mL^{-1} in hexane, Cat.#: E11-10-NPO-HEX-2.5, NanoPartz Inc, Loveland, CO, USA) by 1:20 and 1:7.5 in pure water (Cat.# 320072, Sigma–Aldrich Co., St. Louis, MO, USA) to obtain final nominal NP concentrations of $\approx 4 \times 10^{13}$ NPs mL^{-1} for the experiments described in Figure 2 and $\approx 1 \times 10^{14}$ NPs mL^{-1} for the experiments in Figure 3A and 4.

Imaging: The in situ TEM experiments were performed using a JEOL 2010FEG transmission electron microscope (JEOL Ltd., Tokyo, Japan) operated with an electron accelerating voltage of 200 kV. The movies were acquired at a rate of ten frames per second and a 2×2 binning (1024×1024 pixels) using an ORIUS SC200 CCD camera (Gatan, Inc. Pleasanton, CA, USA). All self-assembly experiments were performed at room temperature. The electron flux for all experiments was maintained at less than $10 \text{ e}^- (\text{\AA}^2 \text{ s})^{-1}$ to reduce the effect of electron beam on the assembly process.^[42,54] TEM images were processed using ImageJ software.^[55] Scanning electron microscopy (SEM) images of the patterned membranes were acquired with an FEI Verios 460 field emission scanning electron microscope (FEI Co., Hillsboro, OR, USA) operated at an accelerating voltage of 3 kV and a landing voltage of 2.5 kV using beam deceleration mode. The probe current used for SEM imaging was 100 pA.

Atomistic MD Simulations: The dodecyl-acrylate-coated gold NPs were modeled using atomistic MD simulations. Each model NP with a hollow gold core with a 7.82 nm diameter was covered by 745 neutral dodecyl acrylate molecules. Two dodecyl-acrylate-coated gold NPs were modeled in a $500 \times 180 \times 240 \text{ \AA}^3$ box. The MD simulations were performed with Nanoscale Molecular Dynamics (NAMD) software package^[56] in the canonical (NVT) ensemble at $T = 300$ K using Langevin dynamics with a damping constant of $\gamma_{\text{Lang}} = 0.1 \text{ ps}^{-1}$ and a time step of 2 fs.

The CHARMM general force field^[57,58] was implemented for the bond, angle and dihedral parameters of the ligands and solvent molecules. Nonbonding interactions between these molecules, such as vdW attraction and steric repulsion, were described by the Lennard–Jones (LJ) potential:

$$U_{\text{LJ}}(r) = \epsilon \left[\left(\frac{r_{\text{min}}}{r} \right)^{12} - 2 \left(\frac{r_{\text{min}}}{r} \right)^6 \right] \quad (1)$$

where ϵ is the minimum (negative) energy of this coupling, and r_{min} is a distance where $U_{\text{LJ}}(r)$ is at a local minimum, which were provided by the CHARMM force field. Here, the r^{-12} term describes the atomic repulsion due to overlapping electron orbitals, and the r^{-6} term represents the vdW attractive coupling. The LJ potential implemented in NAMD has a typical cut-off distance of 1 nm (within the solvent). In vacuum, we extended this distance to 2 nm to provide coupling between the separated NPs in the absence of a connecting medium (solvent).

The electrostatic coupling between ions and partially charged atoms, which also belongs to nonbonding interactions, has a similar cut-off distance as the LJ potential, but its long-range contribution beyond this

cut-off distance was calculated by the PME method^[59] in the presence of periodic boundary conditions.

The bulk vdW interactions between the gold cores of the NPs were separately described (added by us to the CHARMM force field) by the Hamaker formula:^[60]

$$U(D) = -\frac{A}{12} \left(\frac{R}{D \left(1 + \frac{D}{4R}\right)} + \frac{1}{1 + \frac{D}{R} + \frac{D^2}{4R^2}} + 2 \ln \frac{D \left(1 + \frac{D}{4R}\right)}{R \left(1 + \frac{D}{R} + \frac{D^2}{4R^2}\right)} \right) \quad (2)$$

Here, A is the Hamaker constant for the gold–gold interaction in water ($A = 3.0$ eV), $R = 3.91$ nm is the radius of the gold core, and D is the distance between the surfaces of the gold NPs.

Supporting Information

Supporting Information is available from the Wiley Online Library or from the corresponding author.

Acknowledgements

This work was supported by the Singapore Ministry of Education Academic Research Fund Tier 2 (MOE2015-T2-1-007). P.K. acknowledges support from the NSF DMR-1506886 grant.

Conflict of Interest

The authors declare no conflict of interest.

Keywords

in situ transmission electron microscopy, nanochannels, nanoparticles, self-assembly, templated self-assembly

Received: May 14, 2017

Revised: June 19, 2017

Published online: July 28, 2017

- [1] G. M. Whitesides, *Science* **2002**, 295, 2418.
- [2] M. Grzelczak, J. Vermant, E. M. Furst, L. M. Liz-Marzán, *ACS Nano* **2010**, 4, 3591.
- [3] L. Wang, L. Xu, H. Kuang, C. Xu, N. A. Kotov, *Acc. Chem. Res.* **2012**, 45, 1916.
- [4] Z. Nie, A. Petukhova, E. Kumacheva, *Nat. Nanotechnol.* **2010**, 5, 15.
- [5] B. Yan, A. Thubagere, W. R. Premasiri, L. D. Ziegler, L. Dal Negro, B. M. Reinhard, *ACS Nano* **2009**, 3, 1190.
- [6] I. L. Medintz, A. R. Clapp, H. Mattoussi, E. R. Goldman, B. Fisher, J. M. Mauro, *Nat. Mater.* **2003**, 2, 630.
- [7] J. A. Fan, C. Wu, K. Bao, J. Bao, R. Bardhan, N. J. Halas, V. N. Manoharan, P. Nordlander, G. Shvets, F. Capasso, *Science* **2010**, 328, 1135.
- [8] A. Kuzyk, R. Schreiber, Z. Fan, G. Pardatscher, E.-M. Roller, A. Hoge, F. C. Simmel, A. O. Govorov, T. Liedl, *Nature* **2012**, 483, 311.
- [9] X. Wang, D. Liu, S. Song, H. Zhang, *J. Am. Chem. Soc.* **2013**, 135, 15864.
- [10] J. Park, E. Kang, S. U. Son, H. M. Park, M. K. Lee, J. Kim, K. W. Kim, H. J. Noh, J. H. Park, C. J. Bae, J. G. Park, T. Hyeon, *Adv. Mater.* **2005**, 17, 429.
- [11] H. Tan, R. Santbergen, A. H. Smets, M. Zeman, *Nano Lett.* **2012**, 12, 4070.
- [12] P. Reineck, G. P. Lee, D. Brick, M. Karg, P. Mulvaney, U. Bach, *Adv. Mater.* **2012**, 24, 4750.
- [13] N. J. Halas, S. Lal, W.-S. Chang, S. Link, P. Nordlander, *Chem. Rev.* **2011**, 111, 3913.
- [14] B. Willingham, S. Link, *Opt. Express* **2011**, 19, 6450.
- [15] S. A. Maier, P. G. Kik, H. A. Atwater, S. Meltzer, E. Harel, B. E. Koel, A. A. Requicha, *Nat. Mater.* **2003**, 2, 229.
- [16] Y. Min, M. Akbulut, K. Kristiansen, Y. Golan, J. Israelachvili, *Nat. Mater.* **2008**, 7, 527.
- [17] C. A. S. Batista, R. G. Larson, N. A. Kotov, *Science* **2015**, 350, 1242477.
- [18] A. Sánchez-Iglesias, M. Grzelczak, T. Altantzis, B. Goris, J. Pérez-Juste, S. Bals, G. Van Tendeloo, S. H. Donaldson, B. F. Chmelka, J. N. Israelachvili, L. M. Liz-Marzán, *ACS Nano* **2012**, 6, 11059.
- [19] Y. Lalatonne, J. Richardi, M. P. Pileni, *Nat. Mater.* **2004**, 3, 121.
- [20] A. M. Kalsin, M. Fialkowski, M. Paszewski, S. K. Smoukov, K. J. M. Bishop, B. A. Grzybowski, *Science* **2006**, 312, 420.
- [21] K. M. Ryan, A. Mastroianni, K. A. Stancil, H. Liu, A. P. Alivisatos, *Nano Lett.* **2006**, 6, 1479.
- [22] G. Singh, H. Chan, A. Baskin, E. Gelman, N. Repnin, P. Král, R. Klajn, *Science* **2014**, 345, 1149.
- [23] Y. Cai, B.-m. Zhang Newby, *J. Am. Chem. Soc.* **2008**, 130, 6076.
- [24] Z. Nie, D. Fava, E. Kumacheva, S. Zou, G. C. Walker, M. Rubinstein, *Nat. Mater.* **2007**, 6, 609.
- [25] M. A. Correa-Duarte, L. M. Liz-Marzán, *J. Mater. Chem.* **2006**, 16, 22.
- [26] S. Y. Park, A. K. R. Lytton-Jean, B. Lee, S. Weigand, G. C. Schatz, C. A. Mirkin, *Nature* **2008**, 451, 553.
- [27] C. L. Chen, N. L. Rosi, *Angew. Chem., Int. Ed. Engl.* **2010**, 49, 1924.
- [28] Y. Yin, Y. Lu, B. Gates, Y. Xia, *J. Am. Chem. Soc.* **2001**, 123, 8718.
- [29] Y. Cui, M. T. Björk, J. A. Liddle, C. Sönnichsen, B. Boussert, A. P. Alivisatos, *Nano Lett.* **2004**, 4, 1093.
- [30] X. Xiong, P. Makaram, A. Busnaina, K. Bakhtari, S. Somu, N. McGruer, *Appl. Phys. Lett.* **2006**, 89, 193108.
- [31] S. Ni, J. Leemann, I. Buttinoni, L. Isa, H. Wolf, *Sci. Adv.* **2016**, 2, e1501779.
- [32] V. Flauraud, M. Mastrangeli, G. D. Bernasconi, J. Butet, D. T. L. Alexander, E. Shahrabi, O. J. F. Martin, J. Brugger, *Nat. Nanotechnol.* **2017**, 12, 73.
- [33] L. Jiang, X. Chen, N. Lu, L. Chi, *Acc. Chem. Res.* **2014**, 47, 3009.
- [34] T. Kraus, L. Malaquin, H. Schmid, W. Riess, N. D. Spencer, H. Wolf, *Nat. Nanotechnol.* **2007**, 2, 570.
- [35] M. Mastrangeli, *Adv. Mater.* **2015**, 27, 4254.
- [36] E. Rabani, D. R. Reichman, P. L. Geissler, L. E. Brus, *Nature* **2003**, 426, 271.
- [37] T. P. Bigioni, X.-M. Lin, T. T. Nguyen, E. I. Corwin, T. A. Witten, H. M. Jaeger, *Nat. Mater.* **2006**, 5, 265.
- [38] Y. Lin, H. Skaff, T. Emrick, A. D. Dinsmore, T. P. Russell, *Science* **2003**, 299, 226.
- [39] M. J. Williamson, R. M. Tromp, P. M. Vereecken, R. Hull, F. M. Ross, *Nat. Mater.* **2003**, 2, 532.
- [40] H. Zheng, R. K. Smith, Y.-w. Jun, C. Kisielowski, U. Dahmen, A. P. Alivisatos, *Science* **2009**, 324, 1309.
- [41] N. de Jonge, F. M. Ross, *Nat. Nanotechnol.* **2011**, 6, 695.
- [42] U. M. Mirsaidov, H. Zheng, D. Bhattacharya, Y. Casana, P. Matsudaira, *Proc. Natl. Acad. Sci. USA* **2012**, 109, 7187.
- [43] F. M. Ross, *Science* **2015**, 350, aaa9886.
- [44] Y. Liu, X.-M. Lin, Y. Sun, T. Rajh, *J. Am. Chem. Soc.* **2013**, 135, 3764.
- [45] Q. Chen, H. Cho, K. Manthiram, M. Yoshida, X. Ye, A. P. Alivisatos, *ACS Cent. Sci.* **2015**, 1, 33.
- [46] D. A. Welch, T. J. Woehl, C. Park, R. Faller, J. E. Evans, N. D. Browning, *ACS Nano* **2016**, 10, 181.
- [47] E. Sutter, P. Sutter, A. V. Tkachenko, R. Krahn, J. de Graaf, M. Arciniegas, L. Manna, *Nat. Commun.* **2016**, 7, 11213.

- [48] G. Lin, S. W. Chee, R. Sanoj, P. Kral, U. Mirsaidov, *ACS Nano* **2016**, *10*, 7443.
- [49] U. Anand, J. Lu, D. Loh, Z. Aabdin, U. Mirsaidov, *Nano. Lett.* **2016**, *16*, 786.
- [50] G. Lin, X. Zhu, U. Anand, Q. Liu, J. Lu, Z. Aabdin, H. Su, U. Mirsaidov, *Nano. Lett.* **2016**, *16*, 1092.
- [51] J. Park, H. Zheng, W. C. Lee, P. L. Geissler, E. Rabani, A. P. Alivisatos, *ACS Nano* **2012**, *6*, 2078.
- [52] J. Kim, M. R. Jones, Z. Ou, Q. Chen, *ACS Nano* **2016**, *10*, 9801.
- [53] A. Tuteja, W. Choi, M. Ma, J. M. Mabry, S. A. Mazzella, G. C. Rutledge, G. H. McKinley, R. E. Cohen, *Science* **2007**, *318*, 1618.
- [54] S. W. Chee, Z. Baraissov, N. D. Loh, P. T. Matsudaira, U. Mirsaidov, *J. Phys. Chem. C* **2016**, *120*, 20462.
- [55] C. A. Schneider, W. S. Rasband, K. W. Eliceiri, *Nat. Methods* **2012**, *9*, 671.
- [56] J. C. Phillips, R. Braun, W. Wang, J. Gumbart, E. Tajkhorshid, E. Villa, C. Chipot, R. D. Skeel, L. Kalé, K. Schulten, *J. Comput. Chem.* **2005**, *26*, 1781.
- [57] K. Vanommeslaeghe, E. Hatcher, C. Acharya, S. Kundu, S. Zhong, J. Shim, E. Darian, O. Guvench, P. Lopes, I. Vorobyov, A. D. Mackerell, *J. Comput. Chem.* **2010**, *31*, 671.
- [58] W. Yu, X. He, K. Vanommeslaeghe, A. D. Mackerell, *J. Comput. Chem.* **2012**, *33*, 2451.
- [59] T. Darden, D. York, L. Pedersen, *J. Chem. Phys.* **1993**, *98*, 10089.
- [60] J. N. Israelachvili, *Intermolecular and Surface Forces*, Academic Press, San Diego, CA, USA **2011**.